International Journal of Pharmaceutics 410 (2011) 188–195

Contents lists available at ScienceDirect

International Journal of Pharmaceutics

journal homepage: www.elsevier.com/locate/ijpharm

Pharmaceutical Nanotechnology

Physical state and dissolution of ibuprofen formulated by co-spray drying with mesoporous silica: Effect of pore and particle size

Shou-Cang Shen[a,*], Wai Kiong Ng[a], Leonard Chia[a], Jun Hu[a], Reginald B.H. Tan[a,b,*]

[a] Institute of Chemical and Engineering Sciences, A*STAR (Agency for Science, Technology and Research), 1 Pesek Road, Jurong Island, Singapore 627833, Singapore
[b] Department of Chemical and Biomolecular Engineering, The National University of Singapore, 4 Engineering Drive 4, Singapore 117576, Singapore

ARTICLE INFO

Article history:
Received 14 December 2010
Received in revised form 9 March 2011
Accepted 10 March 2011
Available online 16 March 2011

Keywords:
Nanocrystals
Amorphous
Co-spray drying
Mesoporous silica
Dissolution

ABSTRACT

A model poorly aqueous-soluble drug, ibuprofen (IBU), was co-spray dried with mesoporous silica materials having different pore sizes and particle sizes for dissolution enhancement. Drug molecules were entrapped inside the mesoporous channels at a high drug loading of 50:50 (w/w). The pore sizes were found to affect the physical state and particle size of IBU in mesoporous structures, which influenced the dissolution profiles. When IBU was co-spray dried with MCM-41 and SBA-15 with pore size smaller than 10 nm, amorphous state of IBU was obtained due to nano space confinement. In contrast, nanocrystals were obtained when ibuprofen was co-spray dried with large pore SBA-15-LP with pore size above 20 nm. The physical state of ibuprofen played a key role in affecting the dissolution of IBU from the solid dispersion. IBU in the amorphous state exhibited a higher dissolution rate than nanocrystalline IBU, even though the larger pore size could facilitate diffusion from the host matrix. The particle size of mesoporous silica showed a less pronounced effect on the dissolution of IBU. Thus, the amorphous/nanocrystalline state of ibuprofen was the most important influence on drug dissolution followed by the diffusion kinetics, particle size of IBU and path length from host matrix to dissolution medium.

1. Introduction

Since Vallet-Regi et al. (2001) reported the application of MCM-41 mesoporous silica as drug carriers for controlled drug delivery, the utilization of mesoporous silica materials in medicinal formulations has attracted much attention. Because of their stable mesoporous structures, uniform and tunable pore sizes, high silanol-containing surface areas and volumes, easily modified surface features, non-toxic nature, as well as good biocompatibility, mesoporous silica carriers showed advantages over conventional drug carriers for desired drug delivery (Tourné-Péteilh et al., 2003; Barbé et al., 2004; Vallet-Regí et al., 2006; Cariono et al., 2007; Prokopowicz and Przyjazny, 2007; Nunes et al., 2007; Tozuka et al., 2010). Regarding this new application of mesoporous materials, major research focused on the possibility of gaining control over the releasing pattern of the guest drug, which is a critical parameter for clinical applications. Several factors, such as the nature of the host–guest chemical interaction and the pore size of the mesoporous matrix, could affect the release profile of the hosted molecules. Surface functionalized mesoporous MCM-41 has been investigated to create interaction of host–guest for controlled release of various APIs. For instance, amino functional group or other alkaline ingredient modified mesoporous carriers further controlled the release of acidic active molecules by electrostatic interaction (Muñoz et al., 2003; Zhu et al., 2005; Zeng et al., 2006; Song et al., 2005; Shen et al., 2007). On the other hand, carboxyl modified SBA-15 mesoporous materials exhibited pH-responsive delivery for the controlled release of amino-associated drug molecules (Yang et al., 2005; Tang et al., 2006a; Shen et al., 2008). Mesoporous silica has also been functionalized with other functional species to strengthen the control release profiles (Tang et al., 2006b; Yang et al., 2008).

In addition to surface properties, the pore size and particle morphology of porous silica drug carriers have also been found to affect the drug dissolution profile (Aerts et al., 2010). It was reported that the pore size and pore volume of mesoporous dug carriers directly correlated with the drug-loading amount and drug release rate (Izquierdo-Barba et al., 2005; Limnell et al., 2007; Yang et al., 2008; Cauda et al., 2009; Xu et al., 2009; Das et al., 2009). A large pore size usually resulted in a relatively faster drug release in these controlled release systems. Among these reported controlled release systems using mesoporous silica as drug carriers, active ingredients were normally taken up by adsorption (Heikkilä et al., 2007; Thomas et al., 2010). To achieve controlled and sustained release, drug loaded mesoporous silica was pressed to a self-supported disc

* Corresponding author. Tel.: +65 6796 3841; fax: +65 6316 6183.
E-mail addresses: shen_shoucang@ices.a-star.edu.sg (S.-C. Shen), reginald_tan@ices.a-star.edu.sg (R.B.H. Tan).

0378-5173/$ – see front matter © 2011 Elsevier B.V. All rights reserved.
doi:10.1016/j.ijpharm.2011.03.018

for drug release and the disc was usually not disintegrated during the drug release investigation. When drug loaded mesoporous silica was dispersed in a dissolution medium as a powder form, immediate release could be achieved as entrapped drugs easily diffused out of the uniform mesopores (Charnay et al., 2004; Cavallaro et al., 2004; Du and He, 2010). The rapid dissolution of drugs from mesoporous silica has attracted research interest in the formulation of poorly water-soluble drugs to enhance the dissolution rate and bioavailability of such drugs (Salonen et al., 2005; Mellaerts et al., 2007; Wang et al., 2009; Speybroeck et al., 2009). Among different methods used for drug loading, spray drying with mesoporous materials was found to be effective to formulate poorly water soluble drugs with high loading in the amorphous form and the drug dissolution rate was significantly enhanced (Vogt et al., 2008; Shen et al., 2009).

In this study, ibuprofen was chosen as a model compound because of its relatively poor aqueous solubility. Ibuprofen was loaded into mesoporous silica with varied pore structures and particle size via a co-spray drying process to improve its dissolution.

The rate of dissolution (dM/dt) of solid substance can be described by Noyes–Whitney equation:

$$\frac{dM}{dt} = \frac{DS(C_s - C_b)}{h},$$

where M = amount of drug (material) dissolved (usually mg or mmol), t = time (s), D = diffusion coefficient of the drug (cm^2/s), S = surface area (cm^2), h = thickness of the liquid film, C_s and C_b are concentrations of the drug at the surface of the particle (surface = C_s) and the bulk medium (bulk medium = C_b), respectively.

The dissolution rate is directly related to diffusion coefficient of drugs and surface area. For active ingredients formulated with mesoporous silica, it has been reported that the amorphous form exhibited much faster dissolution than the crystal form (Shen et al., 2009). In addition, the pore size and particles size also affect the diffusion coefficient and surface area, thus influencing the dissolution rate. Jin and Liang (2010) reported the effect of the pore size of mesoporous silica at a range of 4.6–7.3 nm on the dissolution behavior of impregnated IBU and observed that the larger pore size facilitated the release of IBU (Limnell et al., 2007; Cauda et al., 2009; Das et al., 2009). In this work, mesoporous silica excipients with pore size range at 2.3–20.1 nm were also studied. The effect of pore size of mesoporous silica on the physical state and the dissolution profiles of IBU was investigated. In addition, the particle size of mesoporous silica also affected the dissolution of IBU as the pathway of IBU diffusion from pore channels varied.

2. Materials and methods

2.1. Materials

MCM-41 with pore size of about 2 nm was prepared by hydrothermal synthesis using cetyltrimethylammonium bromide (CTMABr) as a template. The procedure was as follows: 3.64 g of CTMABr was dissolved in 28.8 g of deionized water, followed by the addition of 9.6 g of sodium silicate solution (35–40%) under stirring. The mixture was adjusted to pH 11 by 2 N HCl solution and transferred to a polypropylene bottle, followed by treatment at 100 °C for 72 h. The resulting white solid was recovered by filtration and dried at 55 °C for 24 h, and finally calcined at 600 °C for 5 h in air at a heating rate of 2 °C/min (Shen and Kawi, 1999).

Submicron mesoporous SBA-15 particles with pore sizes of 6–8 nm were synthesized by a rapid condensation process (Shen et al., 2006). Typically, 4.0 g of EO_{20}–PO_{70}–EO_{20} (P123, pluronic 123, Aldrich) was dissolved in 150 g of 2 N HCl (Kanto Chemical Co. Inc., Japan) solution under stirring at 40 °C for 2 h. 9.0 g of tetraethylorthosilicate (TEOS, Aldrich, 98%) was added to the solution under vigorous stirring for 2 min. The hydrolysis of TEOS was performed at 40 °C for 2 h without stirring. The mole ratio of components in the mixture is SiO_2:P123:HCl:H_2O = 1.0:0.016:6.9:178.6. The mixture was transferred to a polypropylene bottle and aged in an oven at 100 °C for 24 h. The obtained material was filtered and washed with deionized water, then dried at 55 °C for 12 h. To remove the template molecules, the material was heated from room temperature to 550 °C at a heating rate of 2°/min and followed by calcination in air for 6 h.

The large pore SBA-15 (denoted as SBA-15-LP) with pore sizes of 20 nm was synthesized in the presence of mesitylene (1,3,5-trimethylbenzene, TMB, Aldrich) (Nguyena et al., 2008). Typically, TMB is employed to increase the pore size. TMB was added in an equal amount in weight as P123 tri-block polymer to the surfactant solution as the first step of the above described synthesis of SBA-15 particles with pore size of 6 nm. TEOS was then added dropwise to the solution, which was vigorously stirred at 35 °C for 24 h. Finally, the solution was crystallized in a Teflon-sealed autoclave at 110 °C for 72 h. The obtained white solid was recovered and calcined under the same condition as the above described synthesis of SBA-15.

Mesoporous silica nanoparticles (MSN) were prepared using fluorocarbon-surfactant-mediated synthesis as reported by Han and Ying (2005). Typically, 0.5 g of Pluronic P123 and 1.4 g of FC-4 ($(C_3F_7O(CFCF_3CF_2O)_2CFCF_3CONH(CH_2)_3N^+(C_2H_5)_2CH_3I^-$) were dissolved in 80 ml of 0.02 M HCl solution, followed by the introduction of 2.0 g of TEOS under stirring. The solution was continuously stirred at 30 °C for 24 h and then transferred into a polypropylene bottle and kept at 100 °C for 24 h. The resultant solid was recovered by centrifuging and washed with deionized water twice, and then dried at and calcined under the same conditions as above.

Conventional SBA-15 with particle sizes in the tens of micrometers was prepared according to the conventional synthesis procedure (Zhao et al., 1998). The synthesis procedure is identical to that of submicron SBA-15 particles except the hydrolysis of TEOS was conducted under continuous stirring.

Racemic ibuprofen was supplied from Sigma–Aldrich (St. Louis, MO, USA).

2.2. Co-spray drying

1.0 g of ibuprofen was dissolved in 100 ml of ethanol (Fisher Scientific Ltd., UK) and 1.0 g of mesoporous silica was dispersed in the solution under stirring overnight. The spray drying was performed on a BÜCHI B-290 mini spray dryer (BÜCHI Labortechnik AG, Switzerland) operated in inert loop mode with N_2 flow. The inlet temperature was set to 81 °C and the resulting outlet temperature at the above operating condition was approximately 50–55 °C. The feed rate was 4.0 ml/min.

2.3. Differential scanning calorimetry and thermogravimetric analysis

Differential scanning calorimetry (DSC) was performed using a SDT 2960 simultaneous TGA-DSC thermogravimetric analyzer (TA Instrument Co.). 10 mg of sample was used in each experiment. The sample was heated from room temperature to 200 °C under nitrogen flow of 100 ml/min with a heating rate of 10 °C/min. TGA was performed in air-flow and the sample was heated from room temperature to 600 °C. The loading of IBU inside mesoporous silica was determined by the weight loss at temperature range 120–600 °C while all IBU was combusted.

2.4. Powder X-ray diffractometry

Powder X-ray diffraction was performed using a D8-ADVANCE (BRUKER) X-ray diffractometer in steps of 0.02° using Cu Kα

radiation as the X-ray source. The measurement conditions were as follows: target, Cu; filter, Ni; voltage, 40 kV; current, 10 mA; scanning speed, 2°/min.

2.5. Scanning electron microscopy

The particle morphology was examined by high resolution scanning field emission electron microscopy (SEM, JSM-6700F, JEOL, Japan) operating at 5 kV. Prior to analysis, the samples were sputter coated with platinum for 1 min by a sputter coater (Cressington Sputter Coater 208HR, UK).

2.6. Transmission electron microscopy (TEM)

High resolution TEM images were taken by TECNAI F20 (G^2) (FEI, Philips Electron Optics, Holland) electron microscope at 200 kV.

2.7. NMR

Room temperature ^{1}H solid state NMR experiments were conducted with a Bruker FT NMR, DRX-400 MHz instrument operating at a frequency of 400 MHz with 10 s of relaxation delay.

2.8. N_2 adsorption

Nitrogen adsorption/desorption isotherms were measured using an Autosorb-6B gas adsorption analyzer (Quantachrome) at the temperature of −196 °C. Before nitrogen adsorption–desorption measurements, each mesoporous silica sample was heated at 300 °C under vacuum for 3 h and sample loaded with ibuprofen was degassed at 40 °C for 24 h. The specific surface areas of the samples were determined from the linear portion of the Brumauer–Emmett–Teller (BET) plots. The pore size (diameter D_{BET}) distribution was calculated from the adsorption branch of N_2 adsorption-desorption isotherms using the conventional Barrett–Joyner–Halenda (BJH) method. The total pore volume, V_T, was estimated from the amount adsorbed at a relative pressure of 0.95.

2.9. In vitro drug release studies

The dissolution profile of IBU from solid dispersion was measured using a VK7010 (Varian Co) USP dissolution tester with online flow cell Cary 50 UV–vis analysis system (Varian Co., USA). Stirring rate was 100 rpm and the vessel temperature was set at 37 °C. Typically, 50 mg of spray-dried ibuprofen with mesoporous silica (50:50, w/w) and 25 mg of pure ibuprofen crystal were used for dissolution testing in 900 ml of 0.1 N HCl at 37 °C. Samples were taken by auto sampling system equipped with filters at intervals of 5 min. After each measurement, the liquid samples were conveyed back to the dissolution vessels by a peristaltic pump. UV readings were taken at a wavelength of 222 nm.

3. Results and discussion

3.1. Pore structure change after drug loading

Fig. 1 displays the pore size distribution of MCM-41, SBA-15 and SBA-15-LP prior to spray drying with IBU. MCM-41 showed the smallest pore size at 2.3 nm in this study. The uniform pore channels of mesoporous MCM-41 led to a sharp pore size distribution peak as observed in Fig. 1a. The pore size of SBA-15 was about 6 nm. By comparison, the pore size of SBA-15-LP was enlarged to about 20 nm and the pore size distribution peak was broader than that of MCM-41 and SBA-15. Fig. 2 shows the N_2 adsorption/desorption isotherms of MCM-41, SBA-15 and SBA-15-LP, and the isotherms are compared with that spray dried with IBU at 50:50 (w/w). Due to the difference in pore size, MCM-41 showed a N_2 condensation step at P/P_0 of 0.2–0.4, while the condensation step for SBA-15 and SBA-15-LP increased to the ranges of 0.65–0.75, and 0.85–0.95, respectively. After co-spray drying with IBU at ratio of 50:50 (w/w), the N_2 adsorption of IBU/MCM-41 and IBU/SBA-15 dropped to very low level, which corresponded

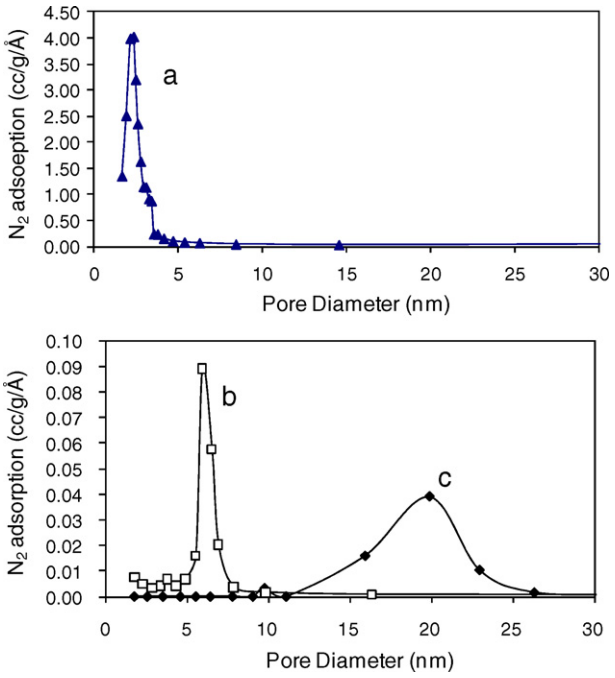

Fig. 1. Pore size distribution of (a) MCM-41, (b) SBA-15 and (c) SBA-15-LP.

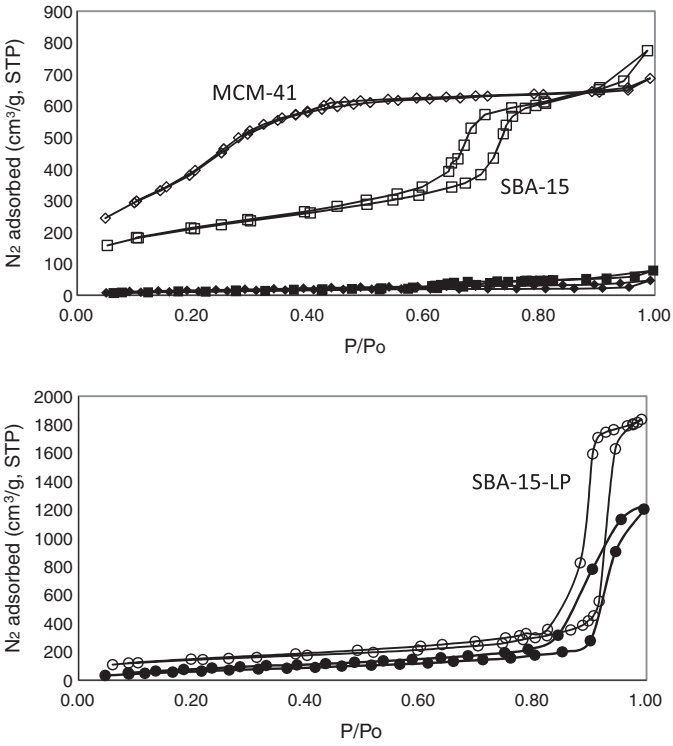

Fig. 2. N_2 adsorption–desorption isotherms of (◊) MCM-41 (♦) IBU/MCM-41 (□) SBA-15, (■) IBU/SBA-15 (○) SBA-15-LP and (●) IBU/SBA-15-LP.

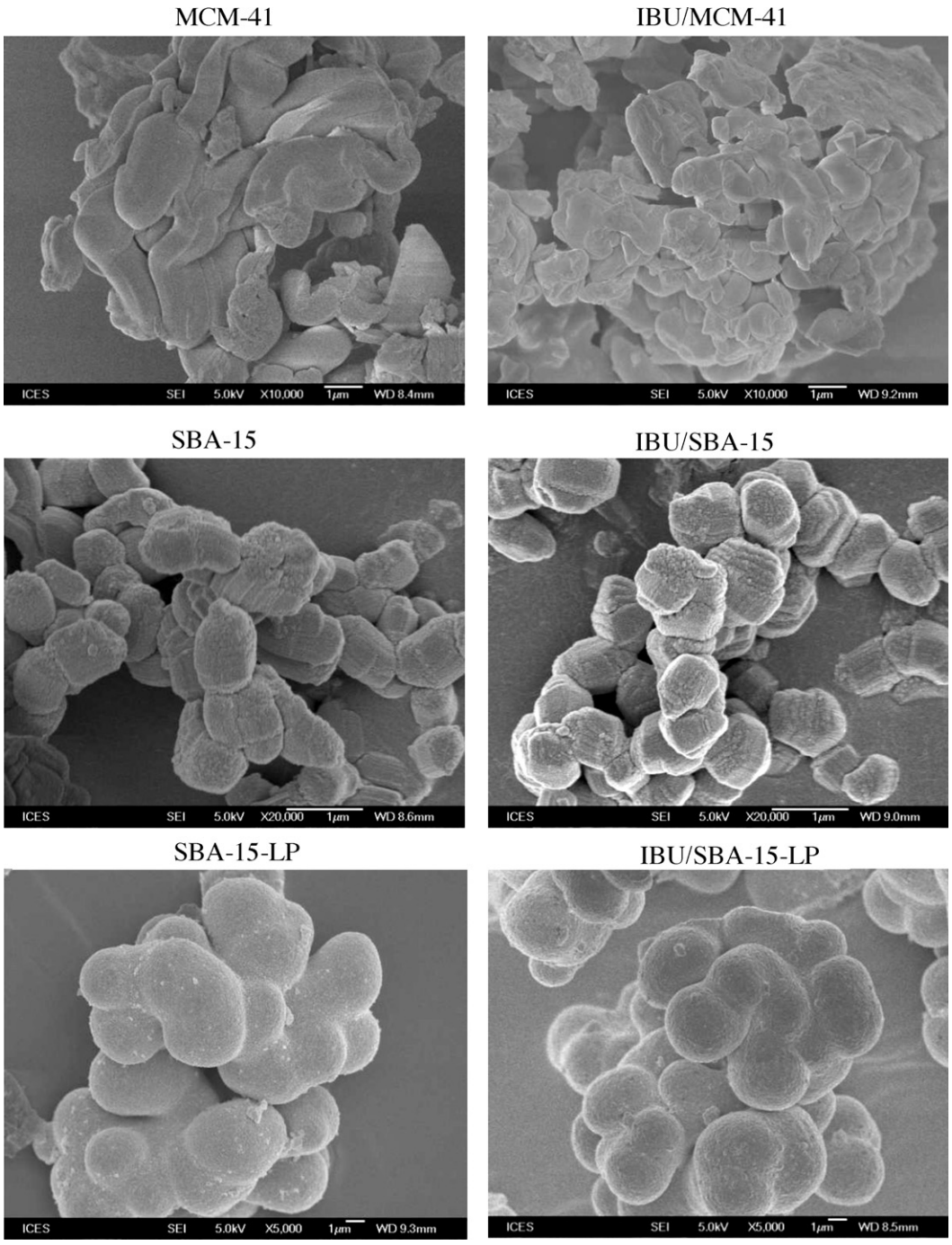

Fig. 3. SEM images of mesoporous silica before and after co-spray drying with IBU (50:50, w/w).

to that of non-porous materials. The results indicated that most of these pore structures were occupied by IBU molecules. As the true density of IBU is 1.076 g/cm^3 and the pore volume of MCM-41 and SBA-15 is 1.0 and 1.05 cm^3/g, respectively, the maximum theoretical loading of IBU inside pore channel of IBU/MCM-41 and IBU/SBA-15 was very close to 50:50 (w/w). Once the pore channels were fully filled, the final solid dispersion was a non-porous material. As shown in Table 1, the pore volume of IBU/MCM-41 and IBU/SBA-15 decreased to 0.04 and 0.09 cm^3/g, respectively. As a comparison, the N_2 adsorption for large pore IBU/SBA-15-LP was not decreased to the base level after co-spray drying. The IBU/SBA-15-LP (50:50, w/w) solid dispersion still possessed pore volume of 1.4 cm^3/g. As the SBA-15-LP material has a large pore volume of 2.94 cm^3/g, the large pore volume was not fully occupied by IBU molecules after the co-spray drying at the ratio of 50:50 (w/w).

3.2. Morphology

Fig. 3 compares the SEM images of three different mesoporous excipients before and after co-spray drying with IBU. The morphology was not obviously changed after spray drying with equal masses of IBU and excipient. As most of IBU was entrapped inside the mesoporous structures within the particles via quick condensation during the rapid spray drying process, only small amount of IBU remained on the external surface of mesoporous parti-

Table 1
Pore structure of mesoporous silica and drug properties of the co-spray dried IBU.

	Specific area (m^2/g)	Pore volume (cm^3/g)	Pore diameter (nm)	Drug loading (%wt.)	Drug states
MCM-41	1363.7	1.0	2.3	–	
IBU-MCM-41	47.33	0.04	–	39.6	Amorphous
SBA-15	734.9	1.05	6.0	–	
IBU-SBA-15	44.3	0.09	–	46.2	Amorphous
SBA-15-LP	531.6	2.94	20.1	–	
IBU-SBA-15-LP	307.2	1.40	17.5	48.3	Amorphous + crystalline

cles. No IBU crystalline particles were observed on the outside of pore channels. The pore volumes of MCM-41, SBA-15 and SBA-15-LP were large enough to accommodate IBU molecules at the moderate 50:50 (w/w) drug loading. The result provided further evidence that most of IBU molecules were entrapped inside the mesoporous channels at different pore size as there was no obvious change to the external morphology of the excipients after drug loading.

3.3. XRD and DSC

Fig. 4 displays XRD patterns of solid dispersion obtained by co-spray dried IBU and mesoporous materials with different pore size. It can be seen that IBU co-spray dried with MCM-41 and SBA-15 exhibited an amorphous state, as no XRD peaks were detected. As expected, crystalline ibuprofen only formed in the larger pores present in SBA-15-LP (Sliwinska-Bartkowiak et al., 2001). Some small XRD peaks due to the IBU nanocrystals could be observed for IBU/SBA-15-LP. The physical state of IBU entrapped in mesoporous structures was also studied by DSC. As seen in Fig. 5, the physical mixture of IBU crystals and SBA-15 (50:50, w/w) exhibited a clear endothermic peak at 78 °C, which is characteristic of the melting of the bulk phase of ibuprofen (Krupa et al., 2010; Tayade and Kale, 2004). The endothermic peak due to the melting of IBU crystals was not observed for IBU/MCM-41 and IBU/SBA-15. The results further confirmed the amorphous state of IBU co-spray dried with SBA-15 and MCM-41, and this was in good agreement with XRD measurement. For IBU/SBA-15-LP, a small endothermic peak was observed at 64.1 °C. Compared with crystal IBU, the co-spray dried IBU/SBA-15-LP showed a significant reduction in the enthalpy of fusion, indicating the decrease in crystallinity of the drug and also suggesting partial amorphous formation (Elkordy and Ebtessam, 2010). The endothermic peak of co-spray dried IBU/SBA-15-LP shifted to a lower temperature, possibly due to interaction of IBU nanoparticles with the surface rich in hydroxyl concentration (Newa et al., 2008) and a significant reduction of particle size to nanoscale.

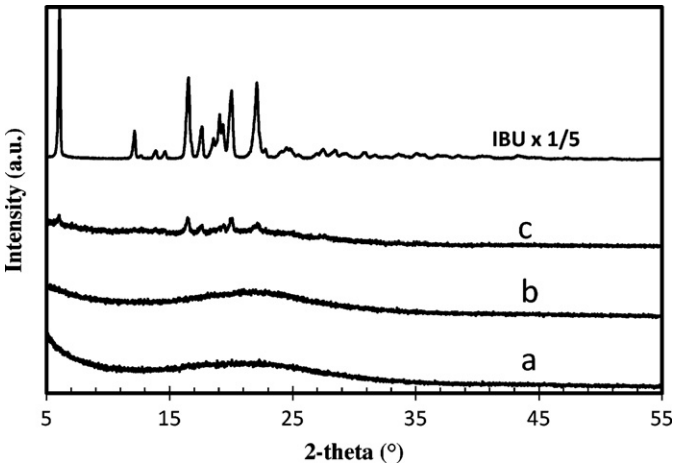

Fig. 4. XRD patterns of (a) IBU/MCM-41, (b) IBU/SBA-15 and (c) IBU/SBA-15-LP.

3.4. ^1H solid-state NMR spectroscopy

Fig. 6 displays ^1H MAS solid-state NMR spectroscopes of IBU co-spray dried with MCM-41, SBA-15 and SBA-15-LP. It is noted that IBU/MCM-41 and IBU/SBA-15 exhibited very good resolution and strong NMR spectra, due to an efficient averaging of the homonuclear ^1H–^1H dipolar interactions coming from the reorientation of IBU within the pore structures (Haeberlen, 1970). As a comparison, the IBU crystals presented a broad line with very low intensity, which is almost not observable when displayed at the same scale with IBU/MCM-41 and IBU/SBA-15. The broad line of ^1H MAS spectroscopy is characteristic of a rigid crystalline solid resulting from the non-complete averaging of the strong homonuclear ^1H–^1H dipolar interaction (Azaïs et al., 2002). The great difference between the IBU/MCM-41 and IBU crystal indicated that the IBU entrapped in the pore channels of MCM-41 and SBA-15 was not in a solid crystal form, which agreed well with the XRD results. Azaïs et al. (2006) investigated IBU entrapped in MCM-41 and found that IBU in the confined space exhibited liquid-like behavior with higher mobility (Tang et al., 2008). The ^1H NMR intensity of IBU/SBA-15-LP is much lower than that of the amorphous IBU/SBA-15 and IBU/MCM-41, as nanocrystals were formed in the large pores of the SBA-15-LP channels. The results indicated that IBU molecules entrapped in MCM-41 and SBA-15 pore channels are extremely mobile at ambient temperature. Although IBU entrapped in SBA-15-LP was crystallized into nanoparticles, the nanocrystalline form in the con-

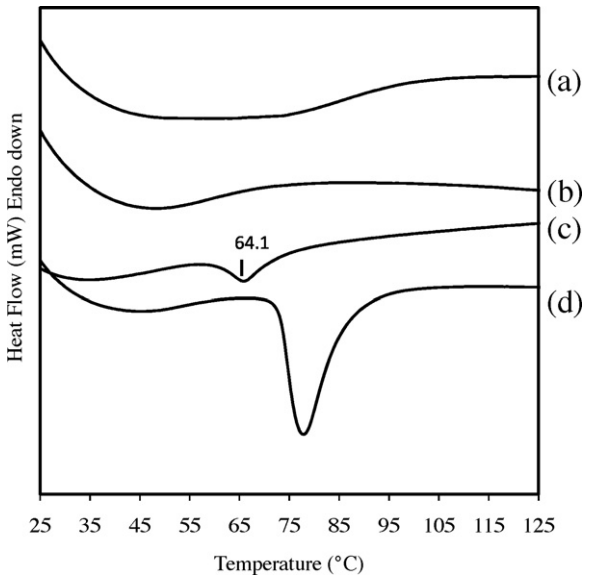

Fig. 5. DSC curves of (a) IBU/MCM-41, (b) IBU/SBA-15, (c) IBU/SBA-15-LP and (d) IBU mixed with SBA-15 (50:50, w/w).

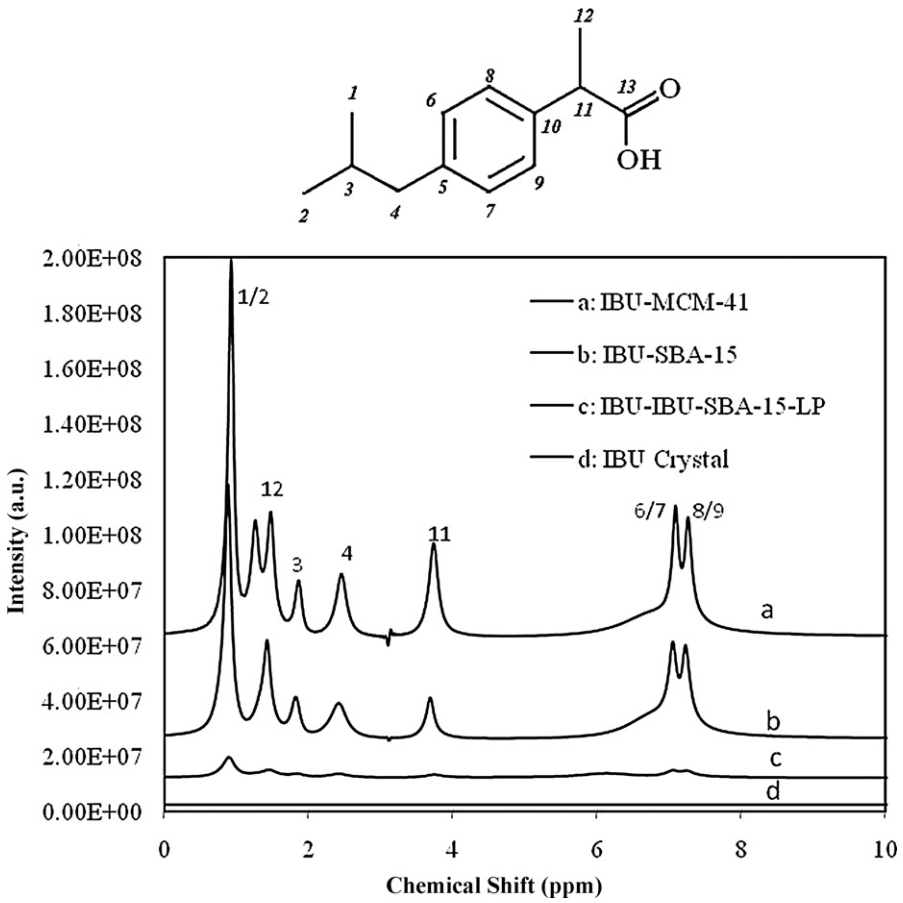

Fig. 6. ^{1}H MAS solid-state NMR spectroscopes of IBU/MCM-41, IBU/SBA-15, IBU/SBA-15-LP and untreated IBU crystal.

fined space still exhibited higher mobility than the untreated IBU crystals.

3.5. Dissolution of IBU from solid dispersion

Fig. 7 displays the dissolution profile of IBU from solid dispersion particles obtained by co-spray drying IBU with MCM-41, SBA-15 and SBA-15-LP, respectively, and compared with untreated IBU crystals (standard error < 3%). The dissolution tests were conducted with the powder form and the solid dispersion was rapidly mixed in the dissolution medium under a paddle stirring rate of 100 rpm.

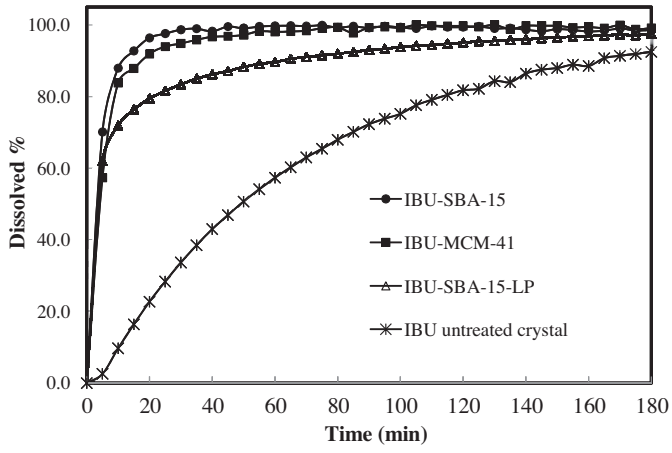

Fig. 7. Dissolution profiles of IBU from IBU/MCM-41, IBU/SBA-15, IBU/SBA-LP and untreated IBU crystal.

It was found that the dissolution rate of co-spray dried IBU/SBA-15 particles was slightly faster than that of IBU/MCM-41. Within the first 15 min, the percentage of IBU dissolved from IBU/SBA-15 solid dispersion reached 95%, while IBU/MCM-41 achieved 88% dissolution. As a comparison, the dissolution of IBU from IBU/SBA-15-LP was slower, with 76% of IBU dissolved in 15 min. As IBU entrapped in both MCM-41 and SBA-15 are in the amorphous form with rapid dissolution property, the pore size appeared to affect the dissolution profiles because the pore size determined the diffusion rate from the pore channels. As the pore size of SBA-15 (~6 nm) was larger than MCM-41 (~2.3 nm), the faster diffusion rate from mesoporous channels of SBA-15 resulted in the higher dissolution rate. However, although SBA-15-LP has much larger pore size than MCM-41 and SBA-15, the dissolution rate of IBU from IBU/SBA-15-LP was slower. The lower dissolution rate of IBU/SBA-15-LP was due to the slower dissolution kinetics of nanocrystalline IBU compared to its amorphous form. Although the large pore size facilitated the diffusion of dissolved molecules from internal pore channels to the dissolution medium, the intrinsic stable crystalline form of IBU in SBA-15-LP exhibited a slower dissolution rate and controls the overall dissolution profile. Nevertheless, the IBU nanocrystal entrapped in mesoporous SBA-15-LP showed a much faster dissolution rate than the original IBU crystal at 16% dissolved in the first 15 min. The three samples of co-spray dried IBU with mesoporous silica materials exhibited excellent dissolution performance due to the amorphous state or the nanocrystalline form with significantly reduced particle sizes that were confined within the mesoporous structures. Especially, those co-spray dried samples showed a similar high immediate release (>50% dissolved) in first 5 min, possibly due to the amorphous or nanocrystalline IBU on surface and near the openings of the pores channels. In addition, the significantly

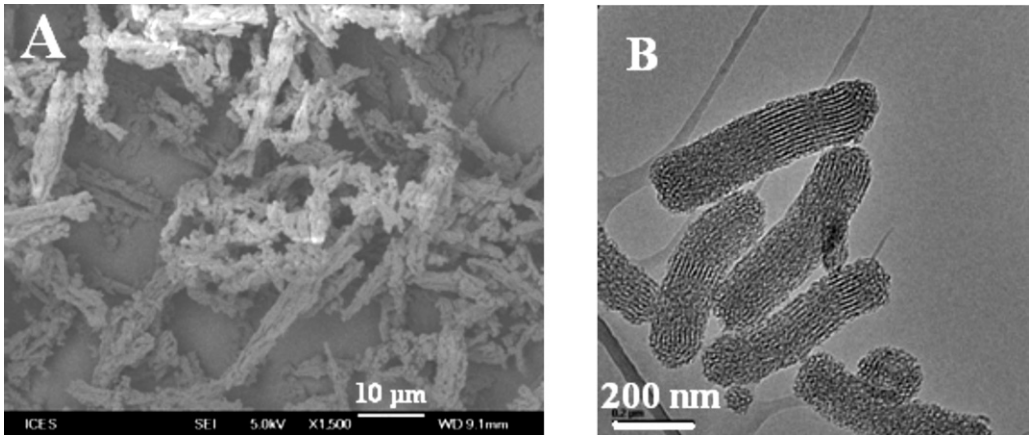

Fig. 8. Morphology of mesoporous silica with different particle size (a) SEM image of conventional SBA-15 large particles and (b) TEM image of mesoporous silica nanoparticles.

reduced particle size of ibuprofen entrapped into pore channels also contributed to the fast dissolution rate of ibuprofen from mesoporous silica matrix.

3.6. Effect of particle size of mesoporous silica

Fig. 8 displays the morphologies of large fiber-like SBA-15 particles and mesoporous silica nanoparticles analyzed by SEM and TEM, respectively. The conventional SBA-15 material (Fig. 8a), which consists of bundles several tens of micrometers in length. As a comparison, the particle size could be also reduced to the nano scale to mesoporous silica nanoparticle (MSN, Fig. 8b). The nanoparticles had a diameter about 150 nm and a length about 300–500 nm. Both mesoporous materials had a very similar pore size of about 6 nm. IBU was loaded onto these two types of mesoporous excipients by co-spray drying with the ratio of 50:50 (w/w). The dissolution profiles of the obtained solid dispersions are shown in Fig. 9. When IBU was co-spray dried with rod-like SBA-15 nanoparticles, the dissolution rate of IBU was higher than that of IBU co-spray dried with fiber-SBA-15 with particle size in tens of microns. The effect of the particle size on the dissolution of IBU was believed to be ascribed to the difference in the length of pore channels. As comparison, the mesoporous silica nanoparticles having short pore channels could further reduce the diffusion resistance for IBU release to the dissolution medium. However, the effect of particle size on dissolution rate is weaker than that of its physical state as shown in Fig. 7, where the dissolution of nanocrystalline form of IBU (IBU/SBA-15-LP) was obviously slower as compared with that of the amorphous form solid dispersion (IBU/MCM-41 and IBU/SBA-15).

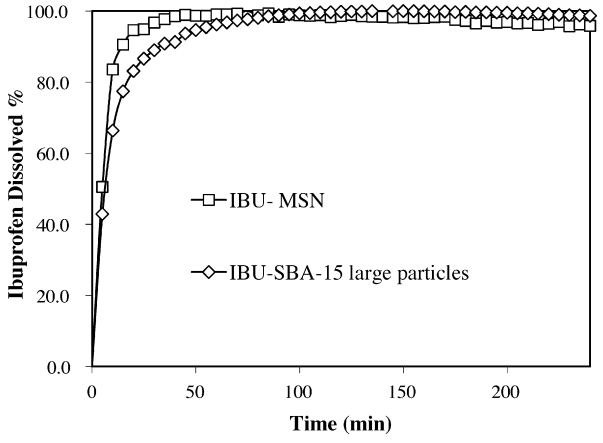

Fig. 9. Dissolution profile of IBU from IBU co-spray dried with conventional SBA-15 large particles and mesoporous silica nanoparticles (MSN).

4. Conclusions

Mesoporous silica materials with varied pore and particle sizes were co-spray dried at high drug loading with a poorly water-soluble model drug (ibuprofen). The obtained solid dispersion significantly enhanced the dissolution rate as compared with the untreated IBU crystal. Among these mesoporous silica loaded IBU, the physical and solid state of ibuprofen were affected by pore size as drug molecules were entrapped inside the confined nano space of mesoporous channels. Nanocrystalline IBU could be formed inside pore channels equal to or larger than 20 nm, while IBU was amorphous in pore size smaller than 10 nm. The dissolution rate was found to be greatly affected by the solid state of ibuprofen. The amorphous IBU exhibited fast dissolution and the rate was weakly affected by pore size variation from 2 to 6 nm. As a comparison, the nanocrystalline IBU in the larger pores of SBA-15-LP possessed a lower dissolution rate, even though the larger pore size could facilitate molecular diffusion from host matrix to medium. The particle size of IBU entrapped into pore channel was determined by pore size and the larger particle size in SBA-15-LP could be one of factors contributing to the slower dissolution than that in SBA-15 and MCM-41. The particle size (ranged from about 150 nm to 20 μm) of SBA-15 only affected the dissolution of IBU slightly, where larger particle size excipients exhibited a slightly slower drug release due to the longer diffusion pathway.

Acknowledgement

This work was generously supported by Institute of Chemical Engineering and Science, Agency of Science Technology and Research, Singapore.

References

Aerts, C.A., Verraedt, E., Depla, A., Follens, L., Froyen, L., Van Humbeeck, J., Augustijns, P., Van den Mooter, G., Mellaerts, R., Martens, J.A., 2010. Potential of amorphous microporous silica for ibuprofen controlled release. Int. J. Pharm. 397, 84–91.

Azaïs, T., Bonhomme-Coury, L., Vaissermann, J., Maquet, J., Bonhomme, C., 2002. The first aluminophosphonate cluster analogue of the 4 = 1 SBU of zeolites: structure and multinuclear solid-state NMR study including 1H NMR. Eur. J. Inorg. Chem. 2002, 2838–2843.

Azaïs, T., Tourné-Péteilh, C., Aussenac, F., Baccile, N., Coelho, C., Devoisselle, J.M., Babonneau, F., 2006. Solid-state NMR study of ibuprofen confined in MCM-41 material. Chem. Mater. 18, 6382–6390.

Barbé, C., Bartlett, J., Kong, L., Finnie, K., Lin, H.Q., Larkin, M., Calleja, S., Bush, A., Calleja, G., 2004. Silica particles: a novel drug-delivery system. Adv. Mater. 16, 1949–1966.

Cariono, I.S., Pasqua, L., Testa, F., Aiello, R., Puoci, F., Iemma, F., Picci, N., 2007. Silica-based mesoporous materials as drug delivery system for methotrexate release. Drug Deliv. 14, 491–495.
Cauda, V., Muhlstein, L., Onida, B., Bein, T., 2009. Tuning drug uptake and release rates through different morphologies and pore diameters of confined mesoporous silica. Micropor. Mesopor. Mater. 118, 435–442.
Cavallaro, G., Pierro, P., Palumbo, F.S., 2004. Drug delivery device based on mesoporous silicate. Drug Deliv. 11, 41–46.
Charnay, C., Bégu, S., Tourné-Péteilh, C., Nicole, L., Lerner, D.A., Devoisselle, J.M., 2004. Inclusion of ibuprofen in mesoporous templated silica: drug loading and release property. Eur. J. Pharm. Biopharm. 57, 533–540.
Das, S.K., Kapoor, S., Yamada, H., Bhattacharyya, A.J., 2009. Effects of surface acidity and pore size of mesoporous alumina on degree of loading and controlled release of ibuprofen. Micropor. Mesopor. Mater. 118, 267–272.
Du, X., He, J.H., 2010. Regulation role of ibuprofen toward the morphology of porous silica nanospheres during its in situ encapsulation. J. Colloid Interface Sci. 345, 269–277.
Elkordy, A.A., Ebtessam, A., 2010. Dissolution of Ibuprofen from spray dried and spray chilled particles. Pak. J. Pharm. Sci. 23, 284–290.
Haeberlen, U., 1970. High Resolution NMR in Solids Selective Averaging. Academic Press, San Diego.
Han, Y., Ying, J.Y., 2005. Generalized fluorocarbon-surfactant-mediated synthesis of nanoparticles with various mesoporous structures. Angew. Chem. Int. Ed. 44, 288–292.
Heikkilä, T., Salonen, J., Tuura, J., Hamdy, M.S., Mul, G., Kumarc, N., Salmi, T., Murzin, D.Y., Laitinen, L., Kaukonen, A.M., Hirvonen, J., Lehto, V.-P., 2007. Mesoporous silica material TUD-1 as a drug delivery system. Int. J. Pharm. 331, 133–138.
Izquierdo-Barba, I., Martinez, A., Doadrio, A.L., Pérez-Pariente, J., Vallet-Reg, M., 2005. Release evaluation of drugs from ordered three-dimensional silica structures. Eur. J. Pharm. Sci. 26, 365–373.
Jin, Z.W., Liang, H., 2010. Effects of morphology and structural characteristics of ordered SBA-15 mesoporous silica on release of ibuprofen. J. Disper. Sci. Technol. 31, 654–659.
Krupa, A., Majda, D., Jachowicz, R., Mozgawa, W., 2010. Solid-state interaction of ibuprofen and Neusilin US2. Thermochim. Acta 509, 12–17.
Limnell, T., Riikonen, J., Salonen, J., Kaukonen, A.M., Laitinen, L., Hirvonen, J., Lehto, V.P., 2007. Surface chemistry and pore size affect carrier properties of mesoporous silicon microparticles. Int. J. Pharm. 343, 141–147.
Mellaerts, R., Aerts, C.A., Humbeeck, J.V., Augustijns, P., Van den Mooter, G., Martens, J.A., 2007. Enhanced release of itraconazole from ordered mesoporous SBA-15 silica materials. Chem. Commun., 1375–1377.
Muñoz, B., Rámila, A., Pérez-Pariente, J., Díaz, I., Vallet-Regí, M., 2003. MCM-41 organic modification as drug delivery rate regulator. Chem. Mater. 15, 500–503.
Newa, M., Bhandari, K.H., Oh, D.H., Kim, Y.R., Sung, J.H., Kim, J.O., Woo, J.S., Choi, H.G., Yong, C.S., 2008. Enhanced dissolution of ibuprofen using solid dispersion with Poloxamer 407. Arch. Pharm. Res. 31, 1497–1507.
Nguyena, T.P.B., Leeb, J.W., Shima, W.G., Moona, H., 2008. Synthesis of functionalized SBA-15 with ordered large pore size and its adsorption properties of BSA. Micropor. Mesopor. Mater. 110, 560–569.
Nunes, C.D., Vaz, P.D., Fernandes, A.C., Ferreira, P., Romäo, C.C., Calhordo, M.J., 2007. Loading and delivery of sertraline using inorganic micro and mesoporous materials. Eur. J. Pharm. Biopharm. 66, 357–365.
Prokopowicz, M., Przyjazny, A., 2007. Synthesis of sol–gel mesoporous silica materials providing a slow release of doxorubicin. J. Microencapsul. 24, 694–713.
Salonen, J., Laitinen, L., Kaukonen, A.M., Tuuraa, J., Björkqvist, M., Heikkilä, T., Vähä-Heikkilä, K., Hirvonen, J., Lehto, V.P., 2005. Mesoporous silicon microparticles for oral drug delivery: loading and release of five model drugs. J. Control. Release 28, 362–374.
Shen, S.C., Kawi, S., 1999. Improvement of both the acidity and stability of MCM-41 by post-synthesis alumination. Chem. Lett., 1293–1294.
Shen, S.C., Chen, F.X., Chow, P.S., Ponpan, P., Zhu, K.W., Tan, R.B.H., 2006. Synthesis of SBA-15 mesoporous silica via dry-gel conversion route. Micropor. Mesopor. Mater. 92, 300–308.
Shen, S.C., Ng, W.K., Chia, L., Dong, Y.C., Tan, R.B.H., 2009. Stabilized amorphous state of ibuprofen by co-spray drying with mesoporous SBA-15 to enhance dissolution properties. J. Pharmaceut. Sci. 99, 1997–2007.
Shen, S.C., Chow, P.S., Chen, F.X., Tan, R.B.H., 2007. Submicron particles of SBA-15 modified with MgO as carriers for controlled drug delivery. Chem. Pharm. Bull. 55, 985–991.
Shen, S.C., Chow, P.S., Kim, S.G., Zhu, K.W., Tan, R.B.H., 2008. Synthesis of carboxyl-modified rod-like SBA-15 by rapid co-condensation. J. Colloid Surf. Sci. 321, 365–372.
Sliwinska-Bartkowiak, M., Dudziak, G., Gras, R., Sikorski, R., Radhakrishnan, R., Gubbins, K.E., 2001. Freezing behavior in porous glasses and MCM-41. Colloid Surf. A: Physicochem. Eng. Aspects 187–188, 523–529.
Song, S.W., Hidajat, K., Kawi, S., 2005. Functionalized SBA-15 materials as carriers for controlled drug delivery: influence of surface properties on matrix–drug interactions. Langmuir 21, 9568–9575.
Speybroeck, M.V., Barillaro, V., Thi, T.D., Mellaerts, R., Martens, J., Humbeeck, J.V., Vermant, J., Annaert, P., Mooter, G.V.D., Augustijns, P., 2009. Ordered mesoporous silica material SBA-15: a broad-spectrum formulation platform for poorly soluble drugs. J. Pharm. Sci. 98, 2648–2658.
Tang, Q.L., Xu, Y., Wu, D., Sun, Y.H., 2006a. A study of carboxylic-modified mesoporous silica in controlled delivery for drug famotidine. J. Solid State Chem. 179, 1513–1520.
Tang, Q.L., Xu, Y., Wu, D., Sun, Y.H., Wang, J.Q., Xu, J., Deng, F., 2006b. Studies on a new carrier of trimethylsilyl-modified mesoporous material for controlled drug delivery. J. Control. Release 114, 41–46.
Tang, X.P., Ng, N.C., Nguyen, H., Mogilevsky, G., Wu, Y., 2008. The molecular dynamics and melting transition of the confined ibuprofen in titania nanotube studied by NMR. Chem. Phys. Lett. 452, 289–295.
Tayade, P.T., Kale, R.D., 2004. Encapsulation of water-insoluble drug by a cross-linking technique: effect of process and formulation variables on encapsulation efficiency, particle size, and in vitro dissolution rate. AAPS Pharm. Sci. 6, doi:10.1208/ps060112, art 12.
Thomas, M.J.K., Slippera, I., Walunja, A., Jain, A., Favrettob, M.E., Kallinteri, P., Douroumis, D., 2010. Inclusion of poorly soluble drugs in highly ordered mesoporous silica nanoparticles. Int. J. Pharm. 387, 272–277.
Tourné-Péteilh, C., Lerner, D.A., Charnay, C., Nicole, L., Begu, S., Devoisselle, J.M., 2003. The potential of ordered mesoporous silica for the storage of drugs: the example of a pentapeptide encapsulated in a MSU-Tween 80. Chem. Phys. Chem. 4, 281–286.
Tozuka, Y., Sugiyama, E., Takeuchi, H., 2010. Release profile of insulin entrapped on mesoporous materials by freeze–thaw method. Int. J. Pharm. 386, 172–177.
Vallet-Regi, M., Rámila, A., del Real, R.P., Pérez-Pariente, J., 2001. A new property of MCM-41: drug delivery system. Chem. Mater. 13, 308–311.
Vallet-Regí, M., Ruiz-González, L., Izquierdo-Barba, I., Gonzalez-Callbet, J.M., 2006. Revisiting silica based ordered mesoporous materials: medical application. J. Mater. Chem. 16, 26–31.
Vogt, M., Kunath, K., Dressman, J.B., 2008. Dissolution enhancement of fenofibrate by micronization, cogrinding and spray-drying: comparison with commercial preparations. Eur. J. Pharm. Biopharm. 68, 283–288.
Wang, F., Hui, H., Barnes, T.J., Barnett, C., Prestidge, C.A., 2009. Oxidized mesoporous silicon microparticles for improved oral delivery of poorly soluble drugs. Mol. Pharm. 7, 227–236.
Xu, W.J., Gao, Q., Xu, Y., Wu, D., Sun, Y.H., Shen, W.L., Deng, F., 2009. Controllable release of ibuprofen from size-adjustable and surface hydrophobic mesoporous silica spheres. Powder Technol. 191, 13–20.
Yang, P.P., Quan, Z.W., Lu, L.L., Huang, S.S., Lin, J., 2008. Luminescence functionalization of mesoporous silica with different morphologies and applications as drug delivery systems. Biomaterials 29, 692–702.
Yang, Q., Wang, S.C., Fan, P.W., Wang, L.F., Di, Y., Lin, K.F., Xiao, F.S., 2005. pH-responsive carrier system based on carboxylic acid modified mesoporous silica and polyelectrolyte for drug delivery. Chem. Mater. 17, 5999–6003.
Zeng, W., Qian, X.F., Yin, J., Zhu, Z.K., 2006. The drug delivery system of MCM-41 materials via co-condensation synthesis. Mater. Chem. Phys. 97, 437–441.
Zhao, D., Feng, J., Huo, Q., Melosh, N., Fredirckson, G.H., Chmelka, B.F., Stucky, G.D., 1998. Triblock copolymer syntheses of mesoporous silica with periodic 50 to 300 angstrom pores. Science 279, 548–552.
Zhu, Y.F., Shi, J.L., Li, Y.S., Chen, H.R., Shen, W.H., Dong, X.P., 2005. Storage and release of ibuprofen drug molecules in hollow mesoporous silica spheres with modified pore surface. Micropor. Mesopor. Mater. 85, 75–81.